International Journal of Mechatronics, Electrical and Computer Technology (IJMEC)
ISSN: 2305-0543 (Online), ISSN: 2411-6173 (Print)
Vol. 11(41), Jul. 2021, PP. 5008-5018

The Effects of Temperature Rise on the Overall Lifespan of Three Phase Induction Motors

Emmanuel Addo
Department of Electrical and Electronic Engineering
Faculty of Engineering
University of Mines and Technology
Tarkwa, Ghana
eaddo@umat.edu.gh

*Erwin Normanyo
Department of Electrical and Electronic Engineering
Faculty of Engineering
University of Mines and Technology
Tarkwa, Ghana
enormanyo@umat.edu.gh

Lawrence Quarshie
Department of Electrical and Electronic Engineering
Faculty of Engineering
University of Mines and Technology
Tarkwa, Ghana
lquarshie29@gmail.com

Abstract— **The operation of a three phase induction motor is accompanied by generation of heat and corresponding temperature rise. This temperature rise increases the frequency of tripping of motor. In extreme cases, there is an increase in cost of operation and maintenance since they are to be replaced or maintained due to burnout. Therefore, this paper explores deeply the effects of temperature on three phase induction motors. The effects of temperature rise are studied theoretically, and hence, an induction motor model was developed in MATLAB/Simulink to mimic the actual nature of the induction motor. In order to achieve the objective of this paper, a thermal model of the induction motor was also developed to represent the thermal behaviours of the induction motor. Simulations of the overall setup were performed and the simulation results were used in determining the effects of temperature rise on the induction motor's performance and service life. Deductions finally made from the predictions indicate that temperature rise has effect on induction motor operation, performance and service life.**

Keywords— ***Induction motor, Modelling, Service life, Simulation, Thermal model***

I. INTRODUCTION

Induction motors just like any machine experience temperature rise during operation. This temperature rise may be due to mere manufacturing or design defects. But far more often, motor overheating problems can be traced to misapplication. Overloading is a leading cause. Frequent tripping are short term symptoms of temperature rise in motors which may be caused by overloading. In extreme cases, motor winding burnout may occur. This may lead to cost of operation by increasing the frequency of repairs or replacement of faulty motors. Major motor component failures and their pecentages are bearings, 41%, stator, 37%, rotor, 10% and accessories, 12% [1-3]. However, according to authors of [4][5], it is known that temperature plays a vital role in the failure of winding insulation and also degradation of bearing lubrication.

Degraded bearing performance arises from lubrication deterioration and contamination, incorrect lubricant viscosity, moisture, vibration, overheating, and electrical pitting [6][7]. The useful life of electric motors is significantly dependent upon the stability of the lubricants. Overheating can result from higher than expected ambient temperatures (above 40 °C) caused by blocked ventilation passages or, more commonly, by overloading the motor. Another form of damage is produced by the existence of potential difference in voltage (ac or dc) between the bearing housing and the shaft due to stray electric currents or unbalanced circuits that may result in the rotor of the machine running at electric potentials different from the stator. Insulation is expected to resist voltage stress as well as to provide mechanical support over a wide range of temperatures under exposure to many environmental factors including oxygen or chemicals in combination with other insulations, without too rapid a rate of degradation so that the desired life may be attained [8-10]. All parts of an electrical equipment do not basically operate at the same temperature. The environment to which a material is exposed strongly affects its heat capability. Finally, the temperature at which one may use a material depends upon the required life of the equipment.

Some related works have been reported in recent times. Gegenava *et al*. [11] evaluated electrical insulation failure of high voltage stator windings of machines by visual inspection of dissected coils and application of Root Cause Analysis (RCA). Authors of [12][13] used the lumped parameter thermal method to conduct thermal performance analysis of the induction motor. Motor temperature was determined at rated load and different values of applied torque at varying stator frequencies. Experimental results gave good accuracy at 3% to 5% error between the measured and calculated temperatures. Thermal effects in high performance electrical machines designed for automotive traction by combining analytical and numerical methods were studied by authors of [14-17]. The heat transfer in electrical machinery was accurately modelled. In [18], authors used mechanical tests to research into ageing and degradation of electrical machines and they stated that the loss factor of machine increases more in the case of circular stresses especially at the exit of the bars from stator slots. Also, class B insulation materials (which generally age quite slowly) performed better than class A materials. Kumari and Gupta [19] looked at the effects of rotor materials and air gap length on the performance of

Article History:
Received Date: Feb. 11, 2021, Accepted Date: Jun. 19, 2021, Available Online: Jul. 01, 2021

different induction motors. Copper cage rotor motors were 5% more efficient compared to the aluminum type. Also, heat load and excitation current increase with increases in air gap length. Authors of [20][21] studied the effect of temperature rise on induction motor performance by way of simulations and experimental studies. They concluded that motor performance (in terms of insulation resistance, stator current, motor efficiency, loading, slip, input power consumption, motor speed) decreases with increasing winding temperature.

Summarily, studies and analysis on thermal, stator and rotor broken bar, bearing faults, motor performance, energy efficiency improvement, ageing and lifespan of motor insulation had been conducted by researchers. Temperature effects on motor lifespan however, have not been studied and reported. The focus of this paper is to investigate the influence of temperature rise on the lifespan and overall performance of SCIM. The contribution reported in this paper serves as an extension of research on the problems associated with the operational temperature rise of SCIM which is the workhorse of industry. The novelty of this paper is in the use of four models namely, dynamic, thermal, lumped parameter and lifespan models to determine influence of temperature on motor stator insulation life as well as on the bearing lubrication life that constitute lifespan of motor.

The rest of the paper is organised as follows: The dynamic, thermal, lumped parameter and lifespan models of the induction motor are presented in Section 2. Section 3 presents the simulation results and discussion. The conclusions of this paper are given in Section 4.

II. MATHEMATICAL MODELLING

A. Dynamic Model of the Induction Motor

In this paper, the squirrel cage induction motor was adopted for study due to its ruggedness as compared to the slip ring induction motor. Also, the number of Squirrel Cage Induction Motors (SCIMs) in use in industry outweighs that of the slip ring type [22]. The dynamic model of the SCIM is derived by using a two phase motor in direct and quadrature (d-q) axes. The conceptual simplicity obtained with the two sets of windings (that is, one on the stator and the other on the rotor) makes it suitable for this analysis. The Clarke and Park's transformation is used for the transformation of three phase stationary axis model to two phase alpha-beta model and then to transform the stationary axis two phase model to rotating axis of two phase d-q axis model. The three phase stator voltages are transferred to a synchronously rotating reference frame in two phases (d-q axis) which is given by (1) [23].

$$\begin{bmatrix} V_d \\ V_q \\ 0 \end{bmatrix} = \frac{2}{3}\begin{bmatrix} \cos(\omega t) & \cos\left(\omega t - \frac{2\pi}{3}\right) & \cos\left(\omega t + \frac{2\pi}{3}\right) \\ -\sin(\omega t) & -\sin\left(\omega t - \frac{2\pi}{3}\right) & -\sin\left(\omega t - \frac{2\pi}{3}\right) \\ \frac{1}{2} & \frac{1}{2} & \frac{1}{2} \end{bmatrix}\begin{bmatrix} V_a \\ V_b \\ V_c \end{bmatrix} \quad (1)$$

where, V_a is voltage of stator phase a; V_b is voltage of stator phase b; V_c is voltage of stator phase c; V_d is voltage in the d axis; V_q is voltage in the q axis.

For the two phase machine representation, d-q circuit equations for stator and rotor and their variables are given. Equation (2) and Equation (3) are expressions for the stator circuit [22].

$$V_{qs} = R_s I_{qs} + \frac{d}{dt}\psi_{qs} + \omega_s \psi_{ds} \quad (2)$$

$$V_{ds} = R_s I_{qs} + \frac{d}{dt}\psi_{ds} + \omega_s \psi_{qs} \quad (3)$$

where, V_{qs}, V_{ds} is stator voltage in q-axis and d-axis respectively; I_{ds}, I_{qs} is stator current in d-axis and q-axis respectively; Ψ_{qs}, Ψ_{ds} is stator flux in q-axis and d-axis respectively; R_s is stator resistance per phase; ω_s is reference frame angular velocity.

If the rotor is stationary, that is $\omega_r = 0$, then the rotor equations will be similar to Equation (2) and Equation (3). The rotor actually moves at speed ω_r and the d-q axes fixed on the rotor, the rotor moves at a speed $\omega_s - \omega_r$ relative to the synchronously rotating frame. Therefore, the rotor equations are defined by (4) and (5) [22].

$$V_{qr} = R_r I_{qr} + \frac{d}{dt}\psi_{qr} + (\omega_s - \omega_r)\psi_{dr} \quad (4)$$

$$V_{dr} = R_r I_{dr} + \frac{d}{dt}\psi_{dr} - (\omega_s - \omega_r)\psi_{qr} \quad (5)$$

where, V_{qr}, V_{dr} is rotor voltage in q-axis and in d-axis respectively; I_{dr}, I_{qr} is rotor current in d-axis and q-axis respectively; Ψ_{qr}, Ψ_{dr} is rotor flux in q-axis and d-axis respectively; R_r is rotor resistance per phase; ω_r is electrical angular velocity of rotor.

With the dynamic model of the machine, all sinusoidal variables in stationary frame appear to be dc quantities in synchronous frame. Therefore, the flux linkage equations in terms of current are given by (6) to (11).

$$\psi_{qs} = L_s I_{qs} + L_m (I_{qs} + I_{qr}) \quad (6)$$

$$\psi_{qr} = L_r I_{qr} + L_m (I_{qs} + I_{qr}) \quad (7)$$

$$\psi_{ds} = L_s I_{ds} + L_m (I_{ds} + I_{dr}) \quad (8)$$

$$\psi_{dr} = L_s I_{ds} + L_m (I_{ds} + I_{dr}) \quad (9)$$

$$\psi_{qm} = L_m (I_{qs} + I_{qr}) \quad (10)$$

$$\psi_{dm} = L_m (I_{ds} + I_{dr}) \quad (11)$$

where, Ψ_{qm}, Ψ_{dm} is magnetizing inductance in q and d-axis respectively; L_s is stator leakage inductance; L_r is rotor leakage inductance; L_m is mutual inductance.

IEEE Office - SEET Complex, Federal University of Technology, Owerri, Nigeria, https://aeuso.org
EISSN: 2305-0543, PISSN: 2411-6173

The electromagnetic torque relation can be derived from (6) to (11) as (12) [22].

$$T_e = \left(\frac{3}{2}\right)\left(\frac{p}{2}\right)\left(\psi_{ds} I_{qs} - \psi_{qs} I_{ds}\right) \quad (12)$$

where, T_e is electromagnetic torque developed; p is number of poles.

Also, the electromagnetic torque is related to the load torque by the expression given in (13) [22].

$$T_e = T_l + J\frac{d\omega_r}{dt} \quad (13)$$

where, T_l is load torque; J is moment of inertia of rotor.

The stator current and rotor current can be obtained from I_{qs}, I_{ds}, I_{qr} and I_{dr} by the Park's transformation as given by (14) and (15), respectively [23].

$$\begin{bmatrix} I_{sa} \\ I_{sb} \\ I_{sc} \end{bmatrix} = \frac{2}{3}\begin{bmatrix} \cos(\omega t) & \sin(\omega t) \\ \frac{-\cos(\omega t)+\sqrt{3}\sin(\omega t)}{2} & \frac{-\sqrt{3}\cos(\omega t)-\sin(\omega t)}{2} \\ \frac{-\cos(\omega t)+\sqrt{3}\sin(\omega t)}{2} & \frac{\sqrt{3}\cos(\omega t)-\sin(\omega t)}{2} \end{bmatrix}\begin{bmatrix} I_{qs} \\ I_{ds} \end{bmatrix} \quad (14)$$

$$\begin{bmatrix} I_{ra} \\ I_{rb} \\ I_{rc} \end{bmatrix} = \frac{2}{3}\begin{bmatrix} \cos(\omega t) & \sin(\omega t) \\ \frac{-\cos(\omega t)+\sqrt{3}\sin(\omega t)}{2} & \frac{-\sqrt{3}\cos(\omega t)-\sin(\omega t)}{2} \\ \frac{-\cos(\omega t)+\sqrt{3}\sin(\omega t)}{2} & \frac{\sqrt{3}\cos(\omega t)-\sin(\omega t)}{2} \end{bmatrix}\begin{bmatrix} I_{qr} \\ I_{dr} \end{bmatrix} \quad (15)$$

B. Thermal Model of Induction Motor

The operation of the induction machine in the dynamic model generates heat. Temperature rise is as a result of heat loss in the SCIM and these heat losses are functions of bearing friction (frictional losses), air friction during rotation (windage losses), eddy current and hysteresis losses (core losses), and copper (I^2R) losses consisting of stator and rotor copper losses [24-26]. The SCIM under operation experiences variable and fixed or constant losses [27-29]. Variable losses change during operation of the motor and these losses are made up of the stator and rotor copper losses. Copper losses are proportional to the load current. Whenever a load is connected to the induction motor, there is the development of copper loss. These losses increase with increase in load applied to the motor. These losses are grouped into two, namely the stator copper losses and rotor winding losses. The stator copper losses are generated in the stator winding of the motor and it is directly proportional to the supply or stator current. The rotor winding losses are losses generated in rotor. The rotor winding loss can be calculated, since the rotor winding loss is proportional to the rotor current.

The constant or fixed losses do not change with loading or during operation. The losses include the core, mechanical (rotational) and stray losses. The core losses which occur within induction machines are quite constant and that they do not change with the load. The core loss of an induction motor depends on the frequency and the maximum flux density. The core losses contain two components and they are the hysteresis and eddy current losses. Hysteresis losses are as a result of magnetic properties of the core material and it is dissipated in the form of heat. Eddy current losses are as a result of circulating current in the motor core and are dissipated in the form of heat. However, rotor core losses are neglected during running conditions. This is because, the eddy and hysteresis losses of the rotor are dependent on frequency of rotor currents. The value of slip is always small and normally equal to or less than 0.04 under operating conditions. Therefore, if stator frequency is 50 Hz, the value of the rotor frequency will be (50 × 0.04) Hz which is very small and negligible. Mechanical losses are made up of two forms of losses. These include friction losses in the bearings and wind age losses which are due to air turbulence and shear as the rotor and stator move past each other.

The various losses are expressed using (16) to (21) [27-29] [30-32].

$$P_{scu} = 3I_s^2 R_s \quad (16)$$

$$P_{rcu} = 3I_r^2 R_r \quad (17)$$

$$P_{core} = P_h + P_e \quad (18)$$

$$P_h = k_h B_{max}^{1.6} f^{1.6} \quad (19)$$

$$P_e = k_e B_{max}^2 f^2 \quad (20)$$

$$P_{mech} = P_f + P_w \quad (21)$$

where, P_{scu} is total stator copper loss; P_{rcu} is total rotor copper loss; P_{core} is total core loss; P_h is hysteresis loss due to stator core; P_e is eddy current loss due to circulating currents; P_{mech} is mechanical losses; I_s is single phase stator current; R_s is resistance of stator winding; I_r is single phase rotor current; R_r is resistance of rotor winding; P_h is stator

IEEE Office - SEET Complex, Federal University of Technology, Owerri, Nigeria, https://aeuso.org
EISSN: 2305-0543, PISSN: 2411-6173

core hysteresis loss; P_e is stator core eddy current loss; k_h is hysteresis constant; B_{max} is maximum magnetic flux density; f is supply frequency; k_e is eddy current constant; P_f is frictional loss and P_w is windage loss.

C. Lumped Parameter Model of the Induction Motor

The lumped parameter model simplifies the description of behaviours of spatially distributed physical model into topology consisting of discrete entities that approximate the behaviours of the distributed system under certain assumptions and useful in electrical systems, mechanical systems and heat transfer. In order to perform a lumped parameter model of the induction motor, points (lumps) from where losses are generated, specifically, the stator core, stator winding, the rotor and bearing are selected. These points serve as the lumped model as the insertion of thermocouples into motors for measurement of temperature are normally done at these positions with hot spot temperatures. The lumped system reduces the thermal system to a number of discrete "lumps" or "points" and assumes the temperature difference within the lumped points to be negligible. This approximation is useful to simplify otherwise complex differential heat equations Fig. 1 illustrates parts of SCIM considered in the lumped parameter analysis [33-35].

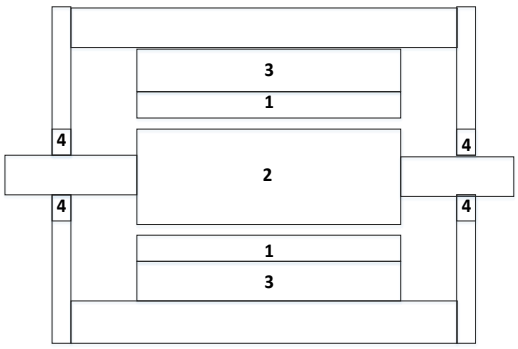

1. Stator winding 3. Stator core
2. Rotor 4. Bearing

Fig. 1 The various heat sources used in the lumped model

If a body is treated as a lumped system heat reservoir, then the total heat content is proportional to product of total heat capacity C, and temperature T. This is indicated in (22) [33-35].

$$Q = CT \tag{22}$$

where, Q is thermal energy; C is thermal capacity; T is temperature. From (22), (23) is obtained.

$$C = \frac{dQ}{dT} \tag{23}$$

Differentiating Equation (23) with regard to time gives (24) which is valid if temperatures in the object are uniform at any given time [33-35].

$$\frac{dQ}{dt} = C\left(\frac{dT}{dt}\right) \tag{24}$$

Energy balance equation is given by the conversion of heat losses into their corresponding temperature rise. In this case, the heat losses obtained from the motor during operation serves as heat energy source or heat reservoir for selected portions of motor for the lumped model. Therefore, the temperature rise in the stator winding, stator core, rotor winding, and bearings are represented by (25) to (28) [12] [13].

$$C_1 \frac{dT_1}{dt} = P_{scu} \tag{25}$$

$$C_2 \frac{dT_2}{dt} = P_{rcu} \tag{26}$$

$$C_3 \frac{dT_3}{dt} = P_{core} \tag{27}$$

$$C_4 \frac{dT_4}{dt} = P_{mech} \tag{28}$$

where, C_1, C_2, C_3, C_4 is thermal capacity for sections 1, 2, 3 and 4, respectively as indicated in Fig. 1. Integrating the system of equations results in the temperature rise at the various sections of the motor.

D. Lifespan of Induction Motor Model

In terms of lifespan of the induction motor, the bearing life as well as the stator insulation life of the motor are evaluated. This is because the bearing as well as stator insulation serve as the main causes of motor faults [1-3]. The effects of temperature on bearing life as well as stator insulation life are assumed to be solely chemical processes. As a result, the bearing and stator insulation lives are analysed using the Arrhenius relation for chemical processes. The Arrhenius relation for chemical breakdown expressed in the logarithmic form is given by (29) [36-38].

$$\ln L = \ln B + \frac{F}{kT} \tag{29}$$

where, L is life of insulation; B is a constant; Φ is activation energy, T is absolute temperature; k is Boltzmann's constant.

Equation (29) is used to determine the effect of temperature on stator winding insulation life. However, for the life of bearing, Equation (29) is used to determine the effect of temperature on bearing lubricant life. The effect of state of lubricant life on bearing life is further evaluated based on the viscosity of lubricant life at different temperatures. The relation is given by (30) [39][40].

$$L = L_{40}\left(\frac{v}{v_{40}}\right)^2 \tag{30}$$

where, L is life of lubrication at a given temperature; L_{40} is life of lubrication at 40 °C (industry base operating temperature); v is viscosity of lubricant life L at a given temperature; v_{40} is viscosity at 40 °C.

Making v the subject of (30) gives (31) [39][40].

IEEE Office - SEET Complex, Federal University of Technology, Owerri, Nigeria, https://aeuso.org
EISSN: 2305-0543, PISSN: 2411-6173

$$v = \frac{\sqrt{v_{40}^2}}{L_{40}} L \qquad (31)$$

The MATLAB/Simulink representation of the models are shown in Fig. 2, Fig. 3 and Fig. 4. The Simulink model for the investigations of the overall system is shown in Fig. 5. The induction motor was modelled to be operating under light and heavy loading conditions achieved by variation of the load torque. This is because, increased loading is one of the factors which increase the operating temperature of induction motor. Numerical data used in the simulations are given in Table 1 and Table 2.

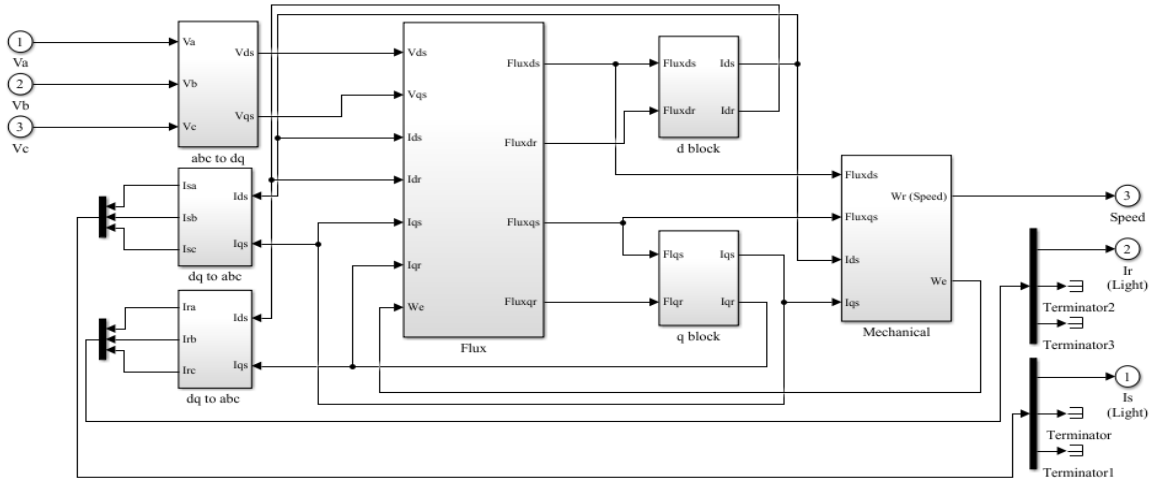

Fig. 2 Induction motor model

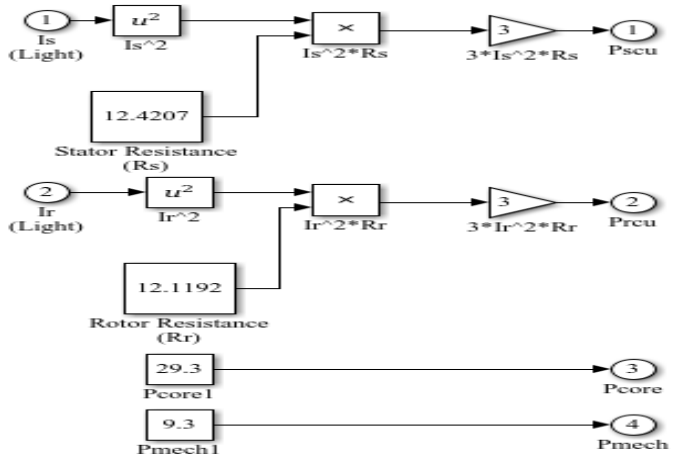

Fig. 3 Heat losses model

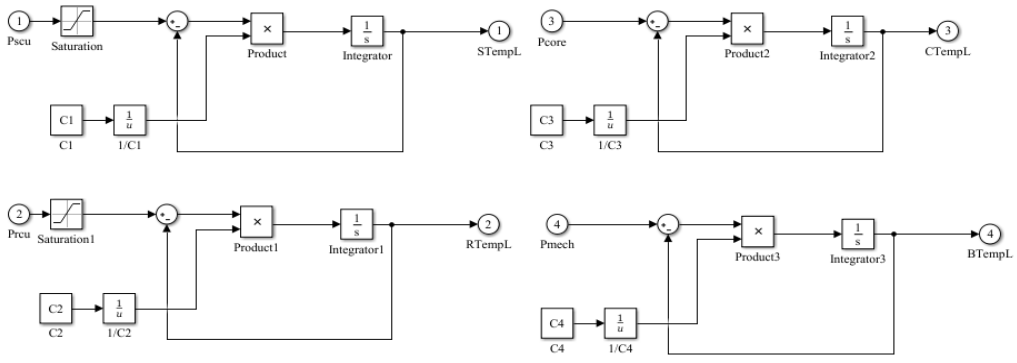

Fig. 4 Temperature estimation model

IEEE Office - SEET Complex, Federal University of Technology, Owerri, Nigeria, https://aeuso.org
EISSN: 2305-0543, PISSN: 2411-6173

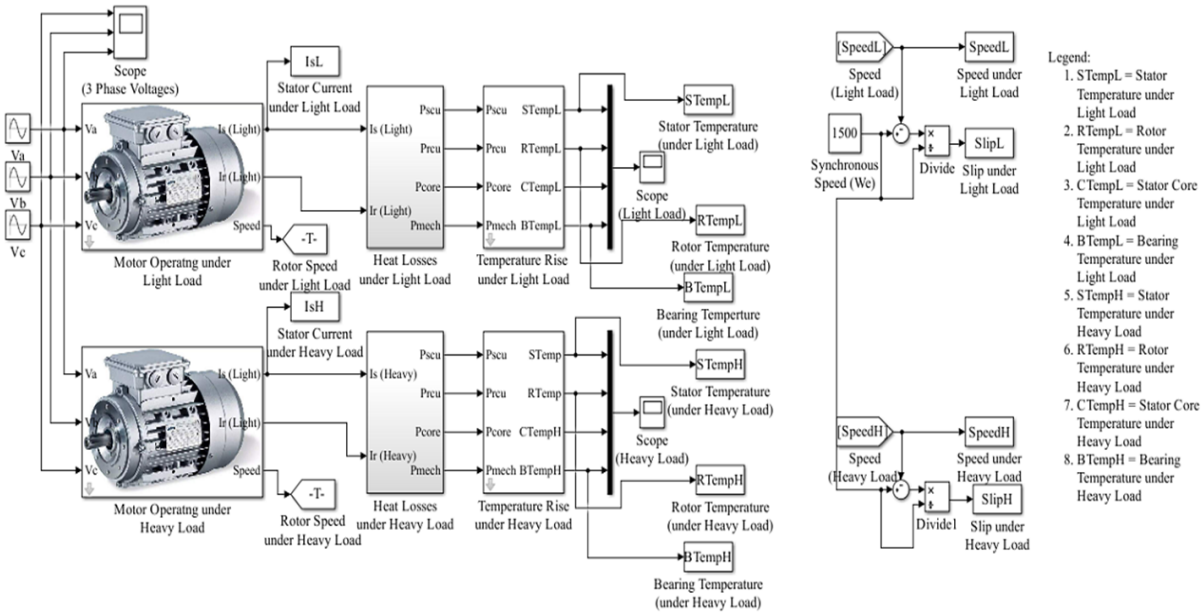

Fig. 5 The overall Simulink model of motor investigation

TABLE 1 INDUCTION MOTOR PARAMETERS

Motor Parameter	**Value**
Rotor Inertia (J) (kgm^2)	0.0088
Power Rating (kW)	0.75
Frequency (f) (Hz)	50
Number of Poles (p)	4
Voltage (V)	220-250/380-415
Speed (ω_r) (rpm)	1390
Iron Loss (at Rated Voltage) (W)	29.3
Mechanical Loss (at Rated Speed) (W)	9.3
Stator Resistance (R_s) (Ω)	12.4207
Rotor Resistance (R_r) (Ω)	12.1192
Stator Inductance (L_s) (H)	1.0245
Rotor Inductance (L_r) (H)	1.0245
Mutual Inductance (L_m) (H)	0.7827

Source: Baranov *et al*. (2021) [41]; Khoury *et al*. (2018) [42]

Kral and Gono (2017) [43].

TABLE 2 THERMAL CAPACITIES OF PARTS OF THE INDUCTION MOTOR

Material	**Thermal Capacity (kJ/kgK)**
Silicon Steel	0.450
Copper	0.385
Aluminium	0.833
Stainless Steel	0.460

Source: Cengel and Ghajar [44]; Karwa [45]

III. RESULTS AND DISCUSSION

A. Simulation Results

The simulation results are presented in Fig. 6 to F

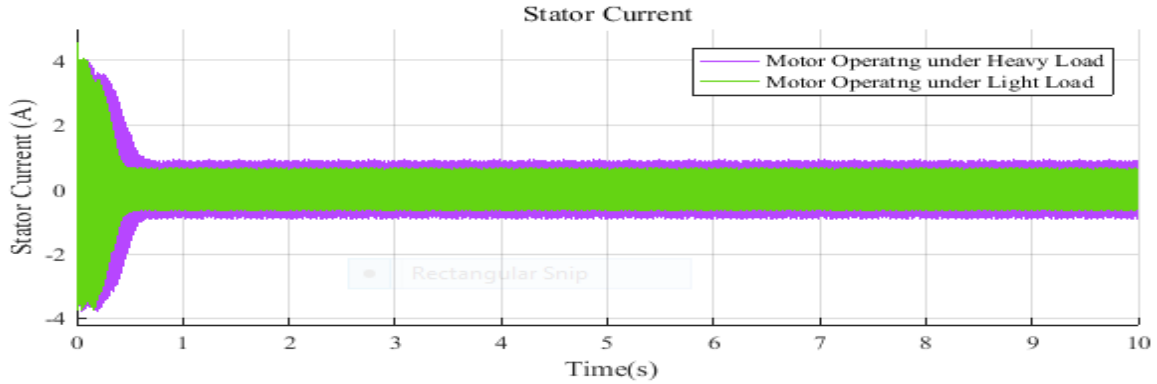

Fig. 6 A graph of stator current versus time under different loads

IEEE Office - SEET Complex, Federal University of Technology, Owerri, Nigeria, https://aeuso.org
EISSN: 2305-0543, PISSN: 2411-6173

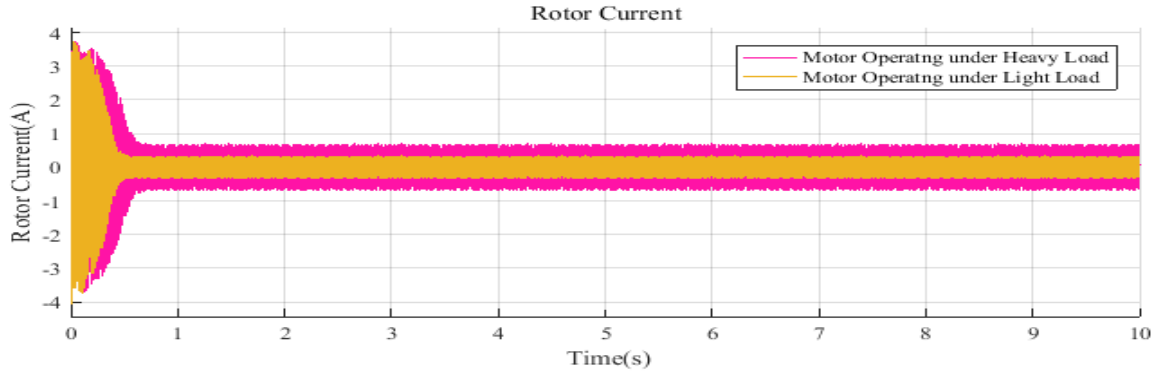

Fig. 7 A graph of rotor current versus time under different loads

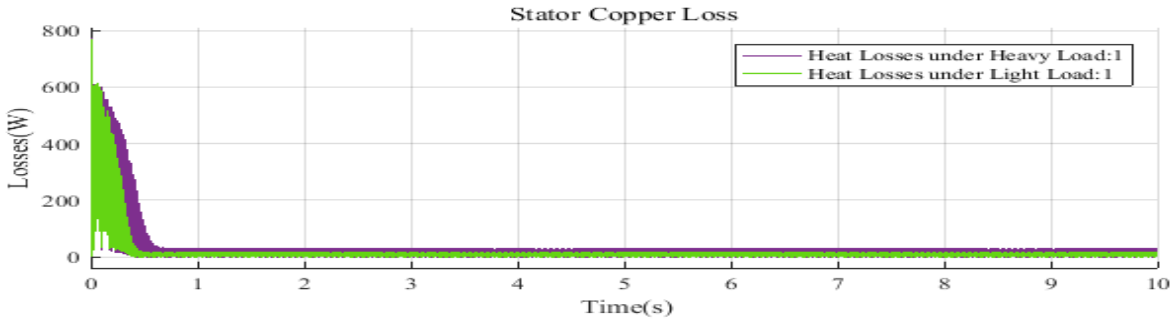

Fig. 8 A graph of stator copper losses versus time under heavy and light loads

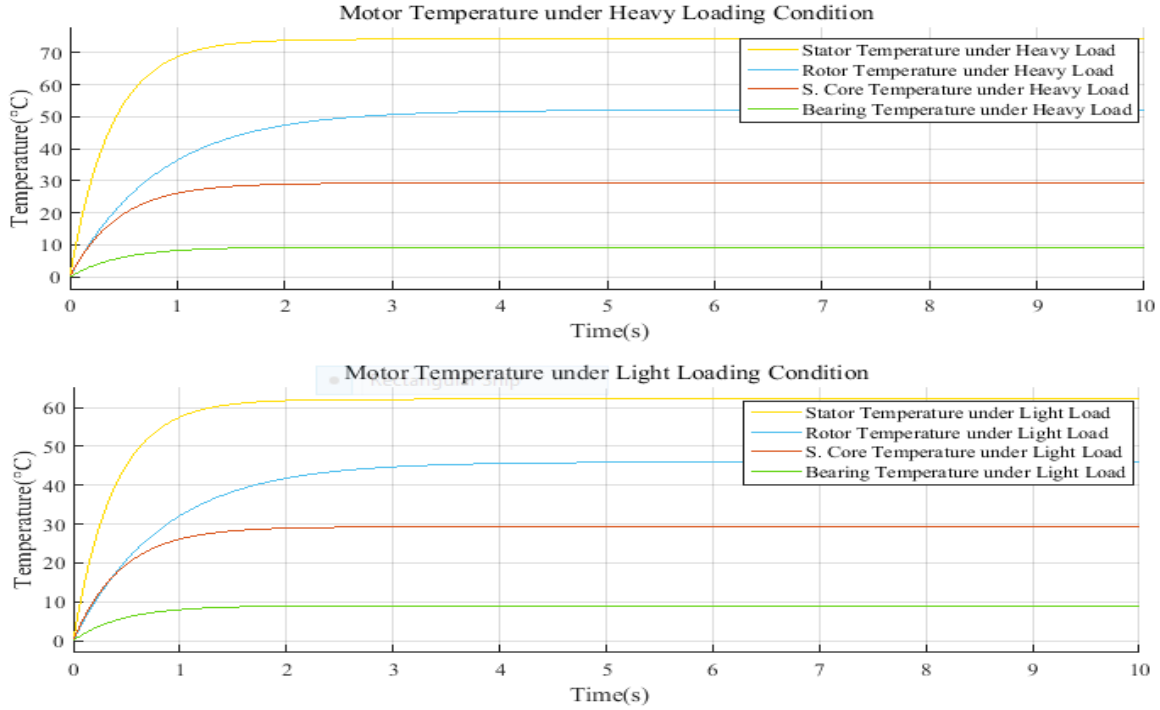

Fig. 9 A graph of temperature rise versus time at different thermal points of motor

IEEE Office - SEET Complex, Federal University of Technology, Owerri, Nigeria, https://aeuso.org
EISSN: 2305-0543, PISSN: 2411-6173

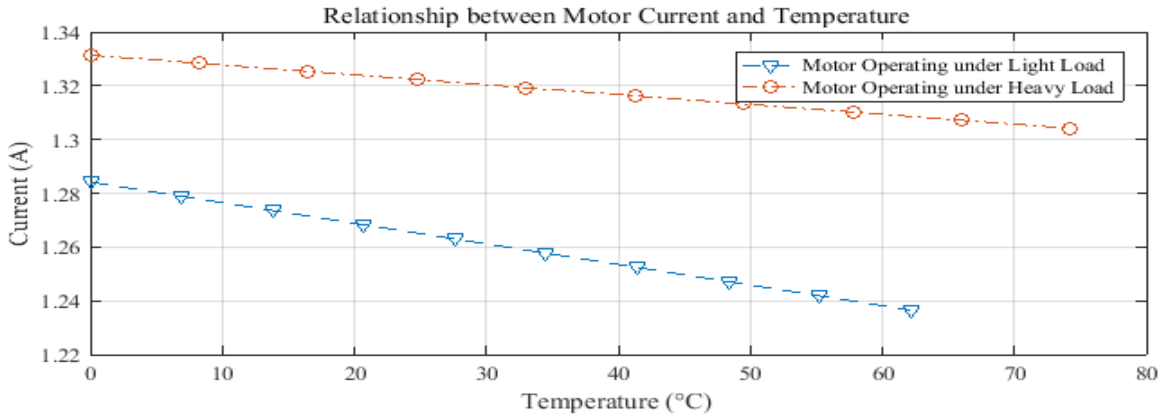

Fig. 10 A graph of stator currents versus temperature

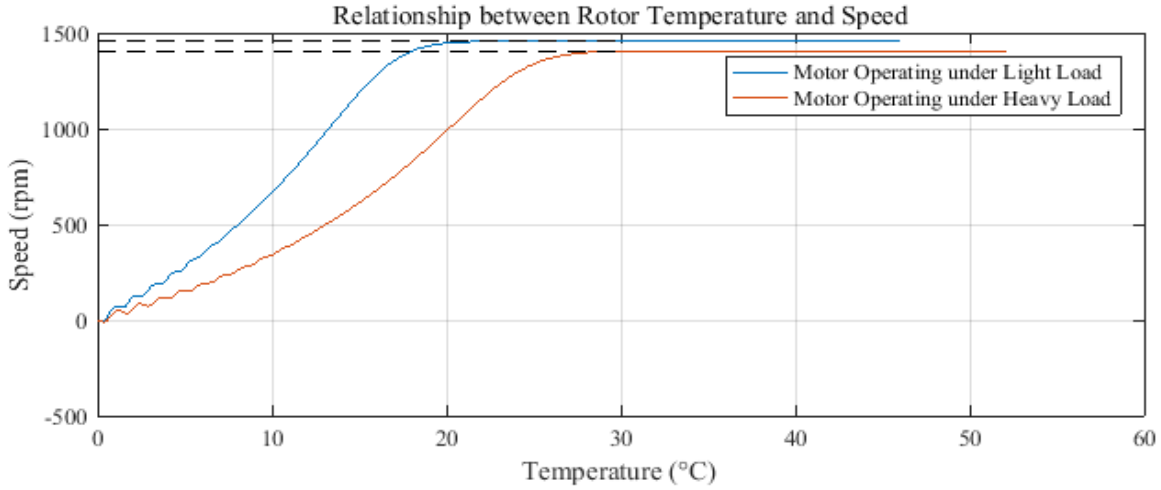

Fig. 11 A graph of motor speed versus temperatures

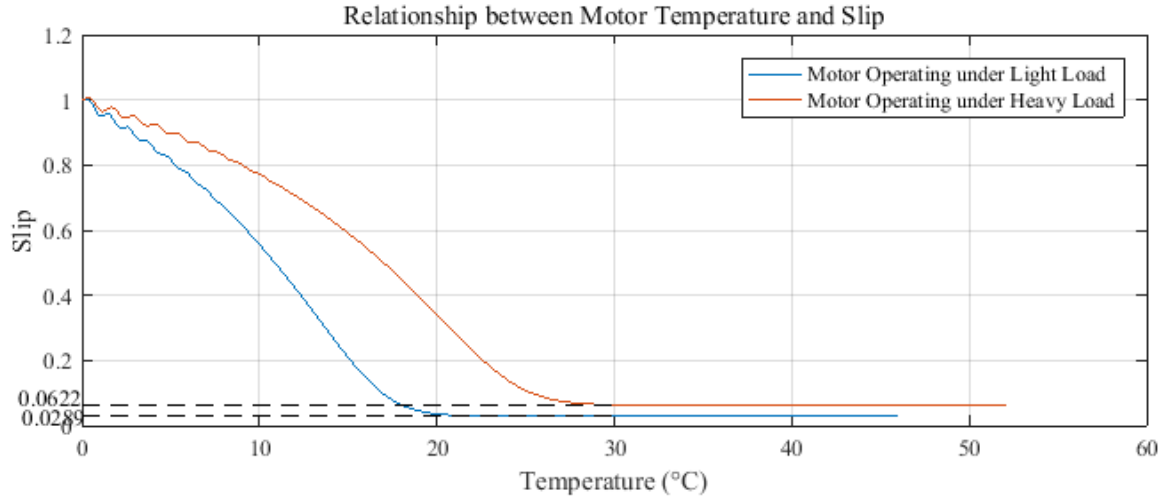

Fig. 12 A graph of motor slip versus temperatures

IEEE Office - SEET Complex, Federal University of Technology, Owerri, Nigeria, https://aeuso.org
EISSN: 2305-0543, PISSN: 2411-6173

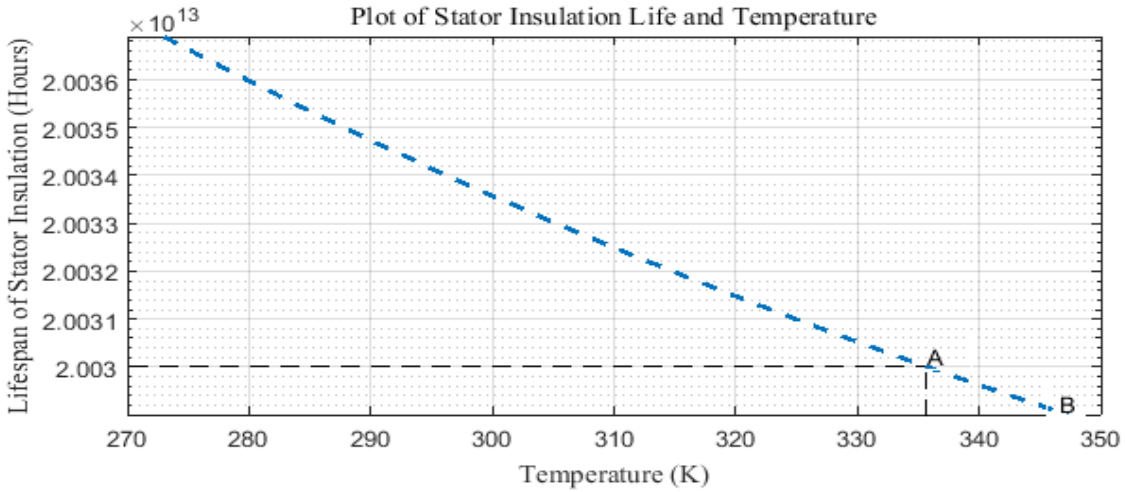

Fig. 13 A graph of stator insulation life versus temperature

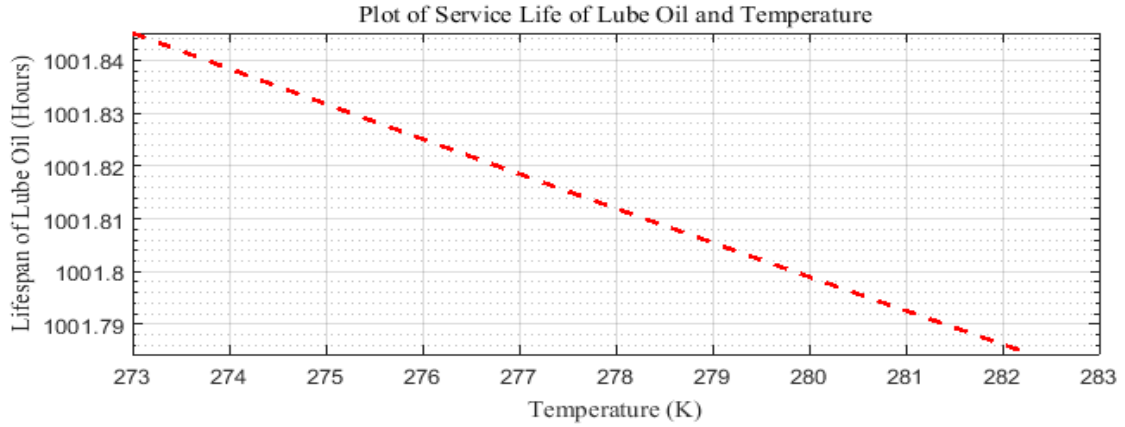

Fig. 14 A graph of lubrication life versus temperature

B. Discussion of Simulation Results

At start, the SCIM stator and rotor currents were the same for both light and heavy loading conditions with a peak of about 4 A. However, from Fig. 6 and Fig. 7, it took about 0.5 s for the stator and rotor currents under heavy load condition to stabilize to a value which was about 0.86 A and 0.70 A, respectively. But with the light loading condition the stator and rotor currents stabilized at about 0.58 A and 0.33 A in 0.3 s, respectively. The peak of stator current at start also confirmed induction motor having high starting current. Comparing the currents, there was a rise from 0.58 A to 0.86 A and 0.33 A to 0.70 A with increase in load as shown in Fig. 6 and Fig. 7, respectively. From Fig. 8, it could be seen that the accompanying losses show similar trend to the currents since losses are proportional to the square of current drawn by the motor due to loading. During the simulations, the temperature at various points within the motor rose to certain limits depending on the quantity of heat produced at those points. The temperatures normalized when the motor achieved a steady state running condition. Comparing the temperature rise recorded for the motor operating under both light and heavy loading condition, it was observed that the heavily loaded motor had higher temperature rise as compared to the case of lightly loaded condition. The comparison between the two conditions in terms of temperature rise is provided in Fig. 9.

The variation of stator currents with temperature is provided in Fig. 10. It can be seen that the increase in temperature did not directly affect the speed of the motor but the applied torque. However, the increase in temperature prolonged the time the motor used in attaining the maximum speed at which the motor operates under a certain load. The speed decreased with increased temperature. This implies that if the temperature becomes extremely high the motor may crawl or seize to rotate. The effect of temperature on motor speed is shown in Fig. 11. From Fig. 12, the decrease in slip increased with temperature before it stabilized at a particular value of slip. Slip took a longer time range to settle under higher temperatures and a lower value when the temperature rise was low. The slip recorded when motor was operating at higher temperature was greater thus, 0.0622 (0.06 %) and low (0.0289 or 0.03%) when operating at lower temperature.

IEEE Office - SEET Complex, Federal University of Technology, Owerri, Nigeria, https://aeuso.org
EISSN: 2305-0543, PISSN: 2411-6173

Stator insulation life decreased with an increase in temperature as could be seen from Fig. 13. At point A on the graph the stator insulation life was estimated to be ≈ 2.003×10^{13} hours when operating temperature was ≈ 335 K ≈ 61.34 °C (under light loading condition). At point B on the graph the stator insulation life decreased to 2.0029×10^{13} hours at operating temperature ≈ 346 K ≈ 73.30 °C (under heavy loading condition). The plot of temperature against lubrication life in Fig. 14 revealed a relationship similar to that of the insulation life. However, the insulation life has a lower activation energy as compared with activation energy of the stator insulation. This is the reason why bearings are to be re-lubricated frequently as compared to stator rewinding. Again, this explains the massive contribution of bearing failure to motor breakdown. The life of a lubricant is proportional to the square of its viscosity (see Equation (30)). As the viscosity of a lubricant decreases, friction and wear increases within the bearing due to uneven lubrication of bearing parts.

IV. CONCLUSION

The bearing lubrication life as well as stator winding insulation life decreased with increase in temperature. Again the performance characteristics of the induction motor operating under higher temperatures are reduced leading to lower efficiency operation due to higher losses. Lubrication of bearing with new lubricant is paramount to control the deterioration of lubrication and reduce failure of the bearing. Consideration must be given to loading of motor as this contributes to motor temperature rise: Increase in loading comes with a corresponding rise in temperature which causes reduction in motor performance in terms of speed, slip and supply current as well as its service life in terms of bearing lubricant life and stator insulation life. For maximum performance as well as increase in service life of motor, motors must be operated with small temperature rise. This means that motors are not to be overloaded beyond their service factor.

REFERENCES

[1] A. Duda and P. Drozdowski, "Induction motor fault diagnosis based on zero-sequence current analysis", *Energies* **2020**, *13*, 6528, pp. 1-25. doi: 10.3390/en13246528. 2020.

[2] J. Tang, J. Chen, K. Dong, Y. Yang, H. Lv and Z. Liu, "Modelling and evaluation of stator and rotor faults for induction motors", *Energies*, **2020**, *13*, 133, pp. 1-20. doi: 10.3390/en13010133. 2020.

[3] M. A. Mohamed, Al-A. A. Mohamed, M. Abdel-Nasser, E. E. M. Mohamed and M. A. M. Hassan, "Induction motor broken rotor bar faults diagnosis using ANFIS-based DWT", *International Journal of Modelling and Simulation*, DOI: 10.1080/02286203.2019.1708173. 2019.

[4] Gundabattini, R. Kuppan, D. G. Solomon et al., "A review on methods of finding losses and cooling methods to increase efficiency of electric machines", *Ain Shams Engineering Journal*, https://doi.org/10.1016/j.asej.2020.08.014, in press.

[5] G. Devarajan, M. Chinnusam and L. Kaliappan, "Detection and classification of mechanical faults of three phase induction motor via pixels analysis of thermal image and adaptive neuro-fuzzy inference system", *Journal of Ambient Intelligence and Humanized Computing*, pp. 1-12, https://doi.org/10.1007/s12652-020-01857-8. 2020.

[6] N. T. Garabedian, B. J. Gould, G. L. Doll and D. L. Burris, "The cause of premature wind turbine bearing failures: Overloading or underloading?", *Tribology Transactions*, Vol. 61, No. 5, pp. 850–859. doi: 10.1080/10402004.2018. 2018.

[7] A. Vencl, V. Gašić and B. Stojanović, "Fault tree analysis of most common rolling bearing tribological failures", *IOP Conf. Ser.: Mater. Sci. Eng.* **174** 012048, pp. 1-10, 2017.

[8] A. Bojovschi, T. V. Quoc, H. N. Trung, D. T. Quang and T. C. Le, "Environmental effects on HV dielectric materials and related sensing technologies", *Applied Sciences*, **2019**, *9*, 856, pp. 1-15. doi:10.3390/app9050856. 2019.

[9] Ghosh and D. Khastgir, "Degradation and stability of polymeric high-voltage insulators and prediction of their service life through environmental and accelerated aging processes", *ACS Omega* 2018, Vol. 3, pp. 11317-11330. *doi: 10.1021/acsomega.8b01560*. 2018.

[10] P. Maussion, A. Picot, M. Chabert, and D. Malec, "Lifespan and ageing modelling methods for insulation systems in electrical machines: A survey", *Proceedings of the 2nd IEEE Workshop on Electrical Machines Design, Control and Diagnostics (WEMDCD'15)*, Turin, Italy, pp. 1-12. doi: 10.1109/WEMDCD.2015.7194541. 2015.

[11] A. Gegenava, A. Khazanov, and P. E. B. Moore, "Failure evaluation for electrical insulation for high voltage stator windings machines and root cause analysis through visual inspection of dissected coils", *Electrical Insulation Conference*, Montreal, Canada, pp. 404–408, 2016.

[12] Adouni and A. J. Marques Cardoso, "Thermal analysis of low-power three-phase induction motors operating under voltage unbalance and inter-turn short circuit faults", Machines **2021**, *9*, 2. Pp. 1-11. https://dx.doi.org/10.3390/machines9010002. 2021.

[13] M. Ojaghi, M. Sabouri and J. Faiz "Performance analysis of squirrel-cage induction motors under broken rotor bar and stator inter-turn fault conditions using analytical modeling", *IEEE Transactions on Magnetics*, Vol. 54, NO. 11, 2018.

[14] B. Li, H. Kuo, X. Wang, Y. Chen, Y. Wang, D. Gerada, S. Worall, I. Stone, Y. Yan, "Thermal management of electrified propulsion system for low-carbon vehicles", *Automotive Innovation*, Vol. 3, pp. 299–316, https://doi.org/10.1007/s42154-020-00124-y. 2020

[15] D. C. Deisenroth and M. Ohadi, **"**Thermal management of high-power density electric motors for electrification of aviation and beyond", *Energies* **2019**, *12*, 3594, pp. 1-18. doi: 10.3390/en12193594. 2019.

[16] W. Liu, Y. Dai, J. Zhao and X. Wang, "Thermal analysis and cooling structure design of axial flux permanent magnet synchronous motor for electrical vehicle", *Proceedings of the IEEE 22nd International Conference on Electrical Machines and Systems (ICEMS)*, pp. 1-6, 2019.

[17] X. Tao, "Design, modelling and control of a thermal management system for hybrid electric vehicles", *Unpublished PhD thesis*, Clemson University, South Carolina, USA, 168 pp. 2016.

[18] C. Rusu-Zagar, P. V. Notingher, and C. Stancu, "Ageing and degradation of electrical machines insulation", *Journal of International Scientific Publications: Materials, Methods and Technologies*, Vol. 8, No. 3, pp. 526–546, 2014.

[19] N. Kumari and A. Gupta, "Effect of various phenomena on induction motor", *International Journal of Research*, Vol. 1, No. 10, pp. 678–681, 2015.

[20] N. V. Irokwe, and O. I. Okoro, "Electrical-thermal coupling of induction machine for improved thermal performance", *Nigerian Journal of Technology*, Vol. 35, No. 4, pp. 912-918, 2016.

[21] N. A. Nour Al-Din, H. A. Ibrahim, S. A. Abdel Maksoud, S. S. Dessouky, "Increased Temperature Effect on Induction Motor Parameters", *Port Said Engineering Research Journal*, Volume 21 No. 1, pp. 109-115, 2017.

[22] S. G. Malla, "A Review on direct torque control of induction motor: with applications of fuzzy - logic", *International Conference on Electrical, Electronic and Optimization Techniques*, Chennai, India, pp. 4557–4567, 2016.

[23] Rimbawati, A. A. Hutasuhut, F. I. Pasaribu, Cholish, Muharnif, "Design of motor induction 3-Phase from waste industry to generator for microhydro at isolated village", *IOP Conf. Series: Materials Science* and *Engineering* **237** 012021, pp. 1-6. doi:10.1088/1757-899X/237/1/012021. 2017.

[24] T. Abdullah and A. M. Ali, "Effect of different ambient factors on temperature distribution in three-phase induction motor", *Journal of Engineering and Sustainable Development*, Vol. 24, No. 02, pp. 48-56, 2020.

[25] F. Santiago, F. Bento, A. J. Marques Cardoso and K. N. Gyftakis, "Thermal analysis of a directly grid-fed induction machine with floating neutral point, operating under unbalanced voltage conditions", *Electric Power Components and Systems*, Vol. 47, No. 11-12, pp. 1060–1076, doi:10.1080/15325008.2019.1659451. 2019.

[26] A. T. Abdullah and A. M. Ali, "Thermal analysis of a three-phase induction motor based on motor-CAD, flux2D, and matlab", *Indonesian Journal of Electrical Engineering and Computer Science*, Vol. 15, No. 1, pp. 46-53, doi: 10.11591/ijeecs.v15.i1.pp. 46-53, 2019.

[27] P. K. Ghosh, P. K. Sadhu, R. Basak and A. Sanyal, "Energy efficient design of three phase induction motor by water cycle algorithm", *Ain Shams Engineering Journal*, Vol. 11, pp. 1139–1147, 2020.

[28] Soomro , M. E. Amiryar, D. Nankoo and K. R. Pullen, **"**Performance and loss analysis of squirrel cage induction machine based flywheel energy storage system", *Appl. Sci.* **2019**, *9*, 4537, pp. 1-26, doi:10.3390/app9214537. 2019.

[29] S. Aryza, M Irwanto, Z. Lubis, A. P. U. Siahaan, R. Rahim, M. Furqan, "A novelty design of minimization of electrical losses in a vector controlled induction machine drive", *IOP Conf. Series: Materials Science and Engineering* **300** 012067, pp. 1-7. doi:10.1088/1757-899X/300/1/012067. 2018.

[30] Ai, C. H. T. Lee, J. L. Kirtley, Y. Huang, H. Wang and Z. Zhang, "A hybrid methodology for analyzing the performance of induction motors with efficiency improvement by specific commercial measures", *Energies* **2019**, *12*, 4497, pp. 1-24. *doi:10.3390/en12234497*. 2019.

[31] M. Altaira, "Efficiency improvement of three phase squirrel cage induction motor by controlling the applied voltage to the stator using simulink models", *MSc Thesis*, Colorado State University, Colorado, USA, 51 pp. 2018.

[32] C. C. Okolo, P. I. Okwu, I. M. Onwusuru, C. S. Uka and K. I. Okolo, " Maximising the Efficiency of 3-Phase Induction Motors (Squirrel Cage Motor)", International Journal for Research in Applied Science & Engineering Technology (IJRASET**),** Vol. 6, Issue IV, pp. 2404-2409. 2018.

[33] D. G. Nielsen, P. R. Andersen, J. S. Jensen and F. T. Agerkvist, "Estimation of optimal values for lumped elements in a finite element – lumped parameter model of a loudspeaker', *Journal of Computational Acoustics*, Vol. 28, No. 2, pp. 1-14. *doi: 10.1142/S2591728520500127*. 2020.

[34] M. Patel, A. Jha1, J. V. S. Harikrishna, R. Trivedi and A. Mukherjee, "Wilkinson type lumped element combiner-splitter for indigenous amplifier development", *IOP Conference Series*: *Journal of Physics: Conference Series* **755** 011001, pp. 1-6. *doi:10.1088/1742-6596/755/1/011001*. 2016.

[35] W. Sun and W. Hu, "Lumped element multimode modelling of balanced-armature receiver using modal analysis", *Journal of Vibration and Acoustics*, Vol. 138, pp. 0610171- 0610178, 2016.

[36] S-H. Lee, T-S. Kong and H.-D. Kim, "Analysis of insulation diagnosis for generator-motor stator winding in pumped storage power plant", *Journal of Electrical Engineering and Technology*, pp. 1-12. *https://doi.org/10.1007/s42835-020-00385-x*. 2020.

[37] M. Lefik, K. Komeza, E. N. Juszczak, D. Roger, P. Napieralski, N. Takorabet, and H. Elmadah, "High temperature machines: topologies and preliminary design", Open Physics, Vol. 17, pp. 657–669, 2019.

[38] B. Silwal and P. Sergeant, "Thermally induced mechanical stress in the stator windings of electrical machines", *Energies* **2018**, *11*, 2113, pp. 1-18. *doi: 10.3390/en11082113*. 2018.

[39] Y. Wang, J. Cao, Q. Tong, G. An, R. Liu, Y. Zhang and H. Yan, "Study on the thermal performance and temperature distribution of ball bearings in the traction motor of a high-speed EMU", *Appl. Sci.* **2020**, *10*, 4373, pp. 1-14. *doi: 10.3390/app10124373*. 2020.

[40] Y. Zhou, R. Bosman and P. M. Lugt, "An experimental study on film thickness in a rolling bearing for fresh and mechanically aged lubricating greases", *Tribology Transactions*, Vol. 62, No. 4, pp. 557–566. *https://doi.org/10.1080/10402004.2018.1539202*. 2019.

[41] G. Baranov, A. Zolotarev, V. Ostrovskii, T. Karimov and A. Voznesensky, "Analytical model for the design of axial flux induction motors with maximum torque density", *World Electric Vehicle Journal*, **2021**, *12*, 24, pp. 1-15. *https://doi.org/10.3390/wevj12010024.* 2021.

[42] W. Khoury, A. Nasser1 and P. Tamás Szemes, "Three phase induction motor modelling and control using vector control in LabVIEW", *MATEC Web of Conferences* **184**, 02019, pp. 1-6, 2018.

[43] M. Kral and R. Gono, "Dynamic model of asynchronous machine*", Proceedings of the 18th International Scientific Conference on Electric Power Engineering (EPE")*, Ostrava, Czech Republic, pp. 1-4, *doi: 10.1109/EPE.2017.7967320*. 2017.

[44] Y. A. Cengel and A. J. Ghajar, *Heat and mass transfer: Fundamentals and applications*, 6th edition, McGraw-Hill Education, New York, USA. 1018 pp. 2020.

[45] R. Karwa, *Heat and mass transfer*, 2nd edition, Springer Nature Singapore Pte Ltd., Singapore. 1147 pp. ISBN: 978-981-15-3988-6 (eBook). 2020.